PAPER

A microfluidic design to provide stable and uniform in-vitro microenvironment for cell culture inspired by the redundancy characteristic of leaf areole†

Jingmin Li,‡[a] Juan Wei,‡[a] Yuanchang Liu,[b] Bo Liu,[c] Tao Liu,[a] Yang Jiang,[a] Laiqian Ding[a] and Chong Liu*[ad]

The leaf venation is considered to be an optimal transportation system with the mesophyll cells being divided by minor veins into small regions named areoles. The transpiration of water in different regions of a leaf fluctuates over time making the transportation of water in veins fluctuate as well. However, because of the existence of multi-paths provided by the leaf venation network and the pits on the walls of the vessels, the pressure field and nutrient concentration in the areoles that mesophyll cells live in are almost uniform. Therefore, inspired by such structures, a microfluidic design of a novel cell culture chamber has been proposed to obtain a stable and uniform microenvironment. The device consists of a novel microchannel system imitating the vessels in the leaf venation to transport culture medium, a cell culture chamber imitating the areole and microgaps imitating the pits. The effects of the areole and pit on flow fields in cell culture chamber have been discussed. The results indicate that the bio-inspired microfluidic device is a robust platform to provide an in-vivo like fluidic microenvironment.

Introduction

Microfluidic technology has many advantages, such as considerable reduction of reagent consumption, continuously fresh media supplying at a controllable flow rate, precise and rapid analyses, etc.[1, 2] It is a crucial tool to provide in-vivo like microenvironment for in-vitro cell culturing.[3-5] However, some challenges still exist in designing a robust microfluidic culture system to mimic the in-vivo microenvironment.[6-8] First, most of the tissue cells live in an interstitial flow environment, where the fluid flows in a constant, stable and slow velocity.[9, 10] Thus, controlling the velocity in the interstitial level is important in the in-vitro culturing of tissue cells. Second, the detected signal of the biochemical reactions in the culture chamber is usually weak.[11, 12] It may be disturbed by the flow fluctuation which may be caused by the variation of temperature, the integration of micropump, microvalve and microsensor, the modification of the surface characteristic etc.[13, 14] Third, the in-vivo medium exchange is achieved through high redundant vascular network[15] which makes the microenvironment for cell growth being stable and uniform. But most of the reported cell culture systems are lack of redundant design, which makes the on-chip microenvironment be different from the in-vivo conditions. Hence, to present a novel microfluidic design which can provide a stable and uniform microenvironment is significant for cell culture, state detection and small-signal extraction.

Some microfluidic systems have been reported to construct the in-vivo like microenvironment. To protect cells from the effect of rapid bulk fluid flow, some microfluidic systems have been designed to isolate the culture chamber from the main channel.[16, 17] By using this design, the medium flows into the chamber mainly by diffusion. The shear stress and the effect of rapid media flow have been avoided. However, the efficiencies of nutrition supply and waste removing in the culture chamber may need to be further improved. To accommodate the effects of rapid media flow, several methods are used to reduce the flow velocities at the locations where the cells residing. Some reports selectively increase the culture chamber depth or the number of the injection channels to allow the perfusion through the chamber ceiling. [18, 19] Others design a special channel network to introduce the flow streams traveling vertically to pass the chambers to reduce the longitudinal flow velocity.[20] Although these special designs are able to reduce the flow velocity, the cells within the culture chamber may still suffer longitudinal or vertical non-specific pressures. A high-aspect-ratio chamber is designed to culture cells with low shear stress.[21] Though this design could provide a uniform supply of medium, the large volume of medium flowing through the culture chamber may induce external disturbance into the chamber. A 3D culture method is presented to use hydrogel to

[a] Key Laboratory for Micro/Nano Technology and System of Liaoning Province, Dalian University of Technology, Dalian, 116023, P. R. China..

[b] Department of Mechanical Engineering, University College London, London, UK, NW12BX.

[c] Department of Biomedical Engineering, Dalian University of Technology, Dalian, 116023, P. R. China.

[d] Key Laboratory for Precision and Non-traditional Machining Technology of Ministry of Education, Dalian University of Technology, Dalian, China.

* Corresponding author Email: chongl@dlut.edu.cn

‡These authors contributed equally to this work.

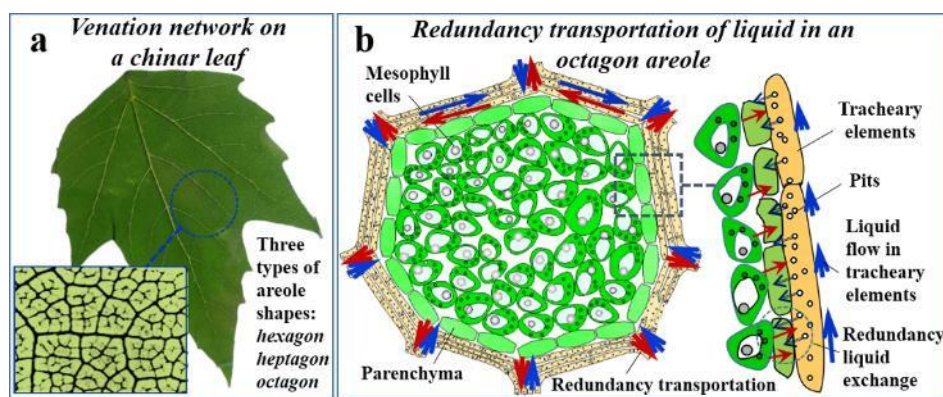†Electronic Supplementary Information (ESI) available: See DOI: 10.1039/x0xx00000x

Fig. 1 The transportation of liquid in an octagonal areole. (a) The areoles on a chinar leaf, which mainly have three kind of shapes, i.e. hexagon, heptagon and octagon. (b) The structure of an octagonal areole and the transportation of liquid in it.

isolate cells from external influences.[22] Due to the porous structure of the collagen-rich system, the flow field distribution may be non-uniform and quantitative analysis may be complicated.

The leaf venation network of dicotyledonous plants has a reticular and hierarchical structure,[23] which is similar to the vascular network in a human body. The network divides a leaf into several small regions named the areoles (Fig. 1a), which contain the mesophyll cells. The shapes of areoles are mainly polygon, especially octagon. For example, the percentages of octagonal areoles in plants of maple, peach, chinar, alamo, sakura and Chinese redbud are 25% - 45%, hexagon and heptagon follow (ESI† Fig. S1). Areoles with more than eight edges also exist. However, the coverage rate and the mechanical property of leaf venation network determine that the proportion of these areoles is very small. The mesophyll cells absorb the liquids and nutrients from the veins in a way that the required liquids are diffused into the surrounding mesophyll cells through the hole-like pits in the cell membranes (Fig. 1b).[24, 25] The most significant characteristic of such a transportation scheme is the 'redundancy' which can be described as follows[26-28]: (1) the hierarchical structure of leaf venation can increase the density of redundant flow paths; (2)more edges of polygonal areoles and more amounts of pits can provide more alternative paths for fluid flowing; (3) the existence of multiple flow paths could be an adaptation to the varying water demands of different parts of the leaf, which could provide a stable microenvironment for the leaf cells. The redundancy is also able to allow a relatively homogeneous liquid supply within an areole, which is capable of maintaining a steady flow pressure and nutrient concentration when the flow rate of the liquid has dramatic changes.[29] Based upon these features, in this paper, by mimicking the redundancy characteristic of the leaf venation network including the hierarchical structure and the polygonal areoles, a microfluidic design which can provide a stable and uniform in-vitro microenvironment for cell culture has been demonstrated.

Principle and design

Principle

The existence of multiple flow paths can make the leaf tolerate damage or adapt to the varying water demands.[28] To describe such a path architecture, redundancy has been used as a parameter to quantify the number of alternative pathways and the level of redundancy of venation networks can be measured by the path distribution[28,30] in a region of interest.

The redundancy is defined as the number of closed polygonal loops per unit area, and the higher the redundancy, the more redundant paths for water to circumvent flow fluctuation.[31] However, when developing such a network, the associated energetic costs and the required amount of materials make the number of loops cannot increase indefinitely in a region of the leaf. In fact, the number of edges in an areole is normally under ten (ESI† Fig. S1). Fig. 2a shows two properties of the minor venation network related to the area of an areole: vein distance (d) and redundancy (R).[31] Distance is defined as the largest inscribed circle diameter of an areole and redundancy is defined as the inverse area of an areole. To simplify the model, we consider the regular polygon.

$$d = a_n \cot(\pi / n) \qquad (1)$$

$$R = 4 / (na_n^2 \cot(\pi / n)) \qquad (2)$$

Where n is the number of edges of a polygon, a_n is the length of the edge. When each areole type has the same vein distance ($d = 1$), R will vary with the number of edges in a regular polygon. As is shown in Fig. 2b, $R = 0.77$ for $n = 3$ and $R = 1.23$ for $n = 10$ reveal that the redundancy of the network increases when the number of edges in a regular polygon is being increased. However, such an increase trend will become less obvious when the number of edges reaches eight with the redundancy being 1.21.

Redundancy can also be expressed by the flow fluctuation within a vein network. We use the path entropy method[32] to establish such a relationship between the flow fluctuation and the redundancy. We consider a uniform network that all the edges have the same flow resistance. First, the redundancy between two nodes a and b in the network is defined as:

$$R = -\sum_{a \in U_b} \frac{q_{ab}}{Q_b} \ln \frac{q_{ab}}{Q_b} \qquad (3)$$

Where q_{ab} is the flow rate from node a to node b, Q_b is the total flow rate into node b, U_b represents a set of nodes at the
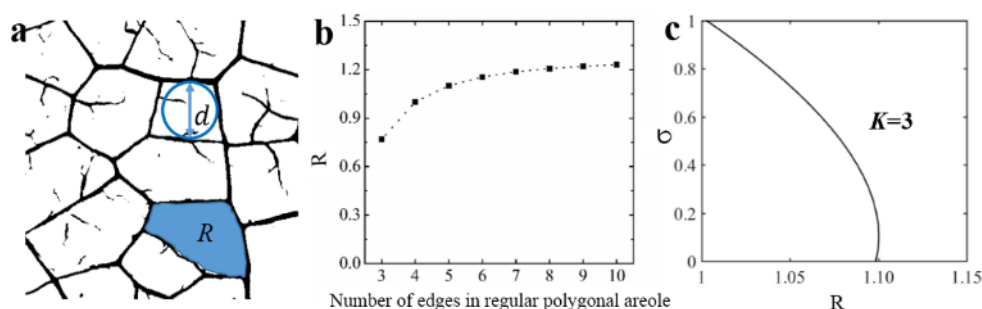
Fig. 2 The traits of minor veins. (a) Venation traits in a certain region of skeletonized image of a leaf. Distance (d) is the inscribed circle diameter of an areole (closed loop). Redundancy (R) is the number of areoles per unit area. (b) Redundancy varies with the number of edges in a regular polygonal areole. (c) The relationship between flow fluctuation coefficient and redundancy.

upstream of node b. We introduce a fluctuation coefficient σ into this network and assume that Q_b is constant. Then R can be expressed as

$$R = -\sum_{i,a\in\overline{u}_b} \frac{(1+\sigma\delta_{ka})f_{ib}}{Q_b} \ln \frac{(1+\sigma\delta_{ka})f_{ib}}{Q_b} \quad (4)$$

Where, δ_{ka} is the Kronecker delta function. As $k=a$, $\delta_{ka}=1$ which means the fluctuation occurs between node a and node b. As $k \neq a$, $\delta_{ka}=0$ which means there is no flow fluctuation. f_{ib} is the flow rate in the branched veins that connecting with node b. We assume the nature material amount of the vein network is a constant and the flows in every branches are all equal to f. If node b has connected with K edges ($K \geqslant 2$), equation (4) can be expressed as

$$R = \frac{(1+\sigma)f}{Q_b} \ln \frac{Q_b}{(1+\sigma)f} + (K-1)\frac{f}{Q_b}\ln\frac{Q_b}{f} \quad (5)$$

As $K = 1$, the flow fluctuation will be directly transmitted from node a to node b. The redundancy R will be equal to zero. Because every braches has a same flow of f and only the sink node has a fluctuation of σf, we assume $f/Q_b \approx 1/K$. Then equation (5) can be simplified as

$$R = \frac{1}{K}\ln\frac{K^{(\sigma+K)}}{(1+\sigma)^{(1+\sigma)}} \quad (6)$$

For most of the leaf venation network, K is equal to 3 and the condition for $K > 3$ is rare. Hence, in this work, we only discuss the condition as $K = 3$. The relationship between redundancy (R) and flow fluctuation coefficient (σ) is shown in Fig. 2c. It can be seen that in a leaf venation network, σ will decrease as R increases. As the redundancy (R) increases to about 1.10, the fluctuation (σ) in the venation network will decrease to 0. This indicates that the external fluid flow fluctuation within the main vein will have limited effects on the flow fields in the minor leaf venation network when the redundancy increases above 1.1, which can provide a steady living environment for the mesophyll cells in the areoles.

Based on the above description, it can be concluded that the increase in the number of edges of an areole will increase the redundancy, which provides alternative routes to accommodate flow fluctuations. As the number of edges of the areoles increases above 6, the redundancy of the network (R) increases above 1.1, the theoretical flow fluctuation within a venation network will becomes very small (near zero). The flow

of water and nutrients to mesophyll tissue under moderate levels of disturbance can be well maintained.

Bionic design of the device

As is shown in Fig. 3, several bio-inspired polygonal chambers have been designed and presented. In order to evaluate their influences on the flow fields in the chambers, several types of chamber shapes, i.e. square, pentagon, hexagon, heptagon, octagon, nonagon as well as decagon, are used for comparison (Fig. 3a and Fig. 3b). All chambers of seven different shapes have been designed to have the same size. A control octagonal device without redundant structures is also used for comparison (ESI† Fig. S9a). In Fig. 3a, three important components of the chamber are presented including the channel structure, cell culture chamber and microgap. The channel structures have been developed by mimicking the hierarchical structures of leaf venation to transport culture medium to the cells and remove the waste. More specifically, the sizes of the channels have been designed by obeying the Murray's law with the main channel having a width of 200 μm and the bifurcated channels having a width of 69 μm. The cell culture chamber mimics the polygonal structure of the areole and the diameter of the inscribed circle being 1000 μm. The microgap between micropillars imitates the pit on the wall of the venation vessel, which is used to transport the culture medium to the cells. The circumferential width of the microgap is 6.25 μm and the radial width is 100 μm. The depths of the chambers, the channels and the microgaps are all 60 μm.

To study the effects on flow fields when adjusting the number of microgaps, a series of chambers with different number of microgaps (i.e. 2, 4, 8, 16, 24, 32, 40 and 48) are designed for experiments (ESI† Fig. S2). Also, to estimate the effects of the size of microgaps, five different sizes, i.e. 5 μm, 6 μm, 7 μm, 9 μm and 11 μm are used in experiments (ESI† Fig. S3). Finally, to consider the influences of the size of chamber, four kinds of chambers with different sizes (their inscribed circle diameters are 500 μm, 1000 μm, 1500 μm and 2000 μm respectively) have been used (ESI† Fig. S4).

Experimental

Device fabrication

The microfluidic device used for experiments is composed of three PDMS layers (Fig. 3c). The top layer is a 1 mm-thick cover
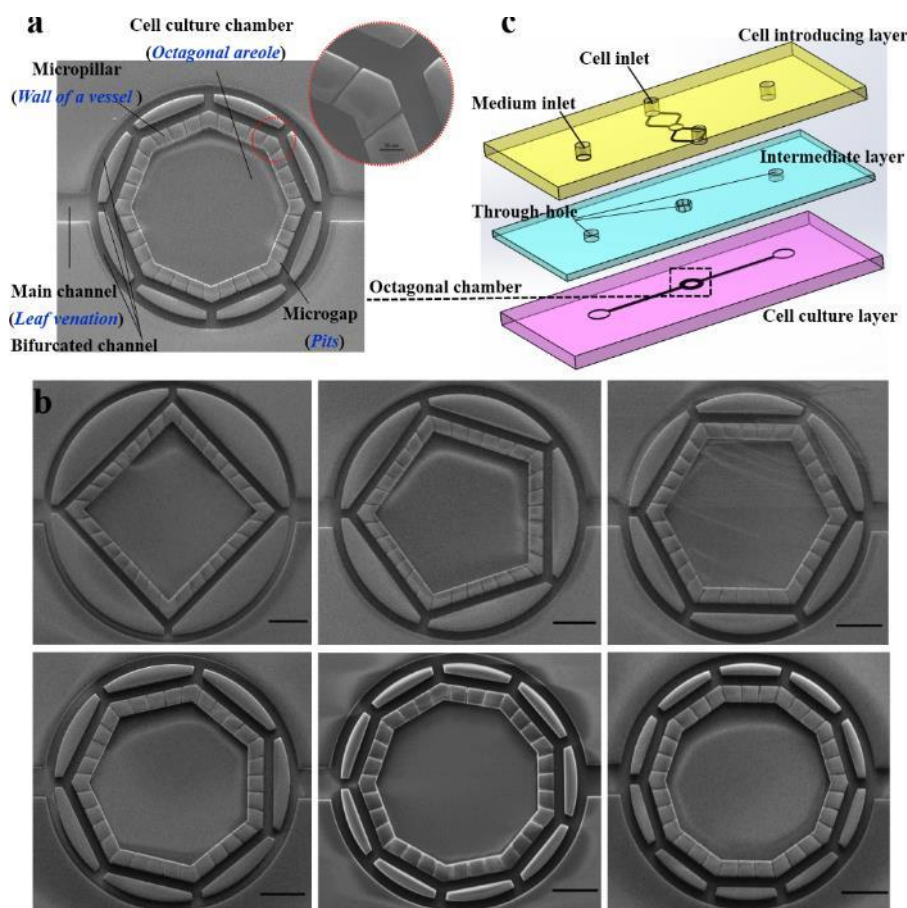
Fig. 3 The shape of cell culture chamber. (a) The bio-inspired octagonal chamber. (b) Six types of chambers with different shapes used as comparison examples. (c) The microfluidic device used to evaluate the performance of the chamber. The scale bar is 300 μm.

plate for cell introducing. The second layer is a 0.5 mm-thick cover plate with three through-holes to connect the top layer with the bottom layer, which is a 1 mm-thick substrate with bio-inspired structures.

The fabrication procedures of the microfluidic devices can be summarized as follows. First, lithographic technique and dry-etching are used to fabricate the silicon mould with the bio-inspired microstructures. The SU-8 moulds are fabricated by using the lithographic technique for cell introducing layer and intermediate layer. Second, the structures on these three moulds are transferred to the PDMS (Sylgard 184, Dow Corning, USA) by using soft-lithography. Third, the medium inlets, medium outlets, cell inlets and cell outlets are punched on cell introducing layers. Finally, after 50 seconds treatment in the oxygen plasma (15 W, 0.08 mbar), the cell introducing layer, the intermediate layer and the cell culture layer are bonded irreversibly on the precise assembling equipment. For the requirement of easily de-moulding of PDMS substrate with microstructures, the three moulds have been put into the trimethylchlorosilane vapor for 30 minutes before being used. In addition, to improve the hydrophilic of PDMS, the deep UV (wave length 255 nm) have been used to enhance the surface energy of the PDMS.

Finite element simulation

To investigate the redundancy transport properties of the bio-inspired devices, the flow fields are simulated using COMSOL Multiphysics Software (version 4.3a, Burlington, MA). The 2D finite element models based on laminar poiseuille flow are developed. To study the stability and uniformity of flow fields in the chambers, the time dependent study and the stationary study of the incompressible Navier-Stokes equation are solved respectively for the carrier liquid to obtain the flow fields. Water under 20°C is selected as the fluid material. As the boundary condition, 6950+2780*sin(π*t) μm/s and 6950 μm/s are set as the inlet velocity respectively for the time dependent study and the stationary study, zero traction and no slip boundary are set at the outlet and on the surface respectively.

Evaluation of flow field in the chamber

To evaluate the flow fields in the chambers, the particle tracking technology is used. The polystyrene (PS) microbeads (Sphere Scientific Co., Ltd., China) with a nominal diameter of 1.33μm and density of 0.95 g/cm³ to 1.05 g/cm³ are selected as the tracking particles. The nominal diameter of the PS microbead is far less than the size of the chambers, the influence of PS microbeads on flow fields can be ignored. The motion of PS microbeads can represent the flowing status of fluids in the chambers. The experimental temperature and humility are 20°C and 50%, respectively. The experiment procedures are summarized as follows. First, the PS microbeads are diluted with deionized water to form a 0.01% suspension. Second, the microfluidic devices are put on the stage of an inverted microscope (Olympus IX71, Japan) and the medium inlets of the

devices are connected to a syringe pump (New Era Pump Systems, Inc. NE-1000, USA) by the silicone tubes. Then, the polystyrene microbeads suspension is perfused into the devices. To study the uniformity of flow field in different chambers, a constant flow rate of 5 µl/min is set on the pump. To investigate the stability of flow fields in different chambers, the constant flow rate of 2 µl/min, 3 µl/min, 5 µl/min and 7 µl/min are set on the pump, respectively. Besides, to imitate the pulsation in the blood vessel, a periodic fluctuation of flow rate is programmed on the pump. Finally, the movements of the microbeads within the chambers are recorded by the CCD camera with an interval of 50ms. The pictures are dealt with Image Pro Plus 6.0 (Media Cybernetics Inc., USA) to draw the trajectories of PS microbeads and calculate their average velocities.

In experiments, the average velocities of 20 PS microbeads that uniformly distributed in the chambers are chosen to represent the velocities in the chambers. Moreover, Brownian motions of PS microbeads can be ignored when compare to the movements driven by the syringe pump. The velocity in the medium inlet can be calculated by Q=A*v, where, Q represents the flow rate, A represents the cross-section area of the microchannel, v represents the average velocity in microchannel.

Cell culture

The Hela cells are purchased from ATCC (Manassas, VA, USA). The PC-12 cells and HUVEC cells are purchased from Cell Bank of the Chinese Academy of Sciences (Shanghai, China). The microfluidic devices and tubes are washed with 75% ethanol and deionized water for three times. After being dried, the devices and tubes are sterilized by high temperature steam and UV light before use. The bottom of the chambers are coated with 5 µg/ml fibronectin (Roche Diagnostics, Indianapolis, USA) and incubated in 37°C for one hour to increase the attachment of cells. Then the device are flushed with PBS to remove the surplus proteins. Before introducing the cells, the medium channels are filled with culture medium to remove the gas in the devices. Besides, to avoid the formation of bubbles, the culture medium droplets are dropped at all the inlets and outlets to isolate the microchannels with atmosphere. The cell suspension at a concentration of 2×10^6 cells/ml is introduced into the chambers from the cell introducing channels and cultured in a 5% CO_2 incubator at 37°C. In order to investigate the effects of the bio-inspired devices on cell culture, the standard culture medium, containing 89% Dulbecco's Modified Eagle Media (DMEM, Gibco, USA), 10% fetal bovine serum (FBS, Gibco, USA), 1% penicillin and streptomycin (PS, Gibco, USA), is used for experiments. The perfusion of the culture medium is started and completed inside the incubator. The microfluidic devices connect to a perfusion system contains 0.8 mm interior diameter silicone tubes, a syringe pump and a 10 mL syringe. The culture medium in the syringe is changed every 24 hours. Flow rate of 5 µl/min is used. The cells are investigated under the inverted microscope (Olympus CKX41, Japan) every 24 hours. The cells are stained by FDA/PI (Live/Dead, Solarbio, Beijing, China).

Statistic

Data are presented as mean ± standard deviation (SD). Differences between two means were determined by the two-tailed unpaired Student's t-test and p < 0.05 were taken as the level of significance.

Results and discussion

Shape effects on flow fields in chamber

To study the influence of chamber shape generated for the uniformity and stability of the flow field in different chambers, the inscribed circle diameters of chambers, the number of microgaps and the size of microgaps of the devices are identical. The velocities in seven types of chamber shapes, i.e. square, pentagon, hexagon, heptagon, octagon, nonagon and decagon, are measured using the particle tracking technique.

Flow behaviour. Polystyrene (PS) microbeads are used as tracking particles and their movements are recorded and analyzed to reveal the flow behaviour in the chambers (Fig. 4a and ESI† Fig. S5). The blue lines in Fig. 4a shows the trajectories of the PS microbeads, which are always in accordance with the fluid streamlines in the chamber (Fig. 4b). Hence, tracking the trajectories of microbeads is able to show the flow field within a chamber. Fig. 4c shows the velocity profile on the line of C-C' and D-D'. It can be observed that the flow velocity exhibits a pronounced reduction after the liquid flows into the chamber through the microgaps; whereas, within the chamber, the flow velocity retains steady. However, as the fluid flows out of the chamber, a dramatic change of the velocity occurs again as a sharp velocity increase can be observed. These phenomenon can also be proved by tracking the trajectories of the microbeads.

Uniformity of flow fields in chamber. A syringe pump is used to inject the suspension containing PS microbeads into the experimental devices with an initial injection flow rate of 5 µl/min (about 6950 µm/s in the medium inlet of the devices) being selected. The velocities of twenty PS microbeads which distribute uniformly in the chambers are shown in Fig. 4d. It can be found that as the number of edges (N_e) in the polygonal chamber increases from 4 to 8, a nearly 64% drop of the maximum velocity within the polygonal chambers occurs when the velocity decreases from 35.0 µm/s to 12.5 µm/s. However, when the number of edges (N_e) is more than 8, such a velocity change becomes slight. The velocity difference in different regions in the polygonal chamber is about 13.0 µm/s when N_e is 4. However, it reduces to about 4µm/s when N_e is more than 8. Such a result indicates that the increase of the number of the edges is able to make the flow fields uniform. To further demonstrate the results, we use standard deviation to evaluate the velocity differences in different regions in the polygonal chambers (Fig. 4e) with the same experiment for each number of edges been repeated four times. It can be seen that, the standard deviation reduces as N_e in the polygonal chambers increase. When N_e is 4, the standard deviation of velocities within a chamber is 3.0 µm/s-3.2 µm/s. When N_e is above 8, the standard deviation reduces about 60% to 1.2 µm/s-1.3 µm/s. The pronounced reductions of velocities and standard deviation
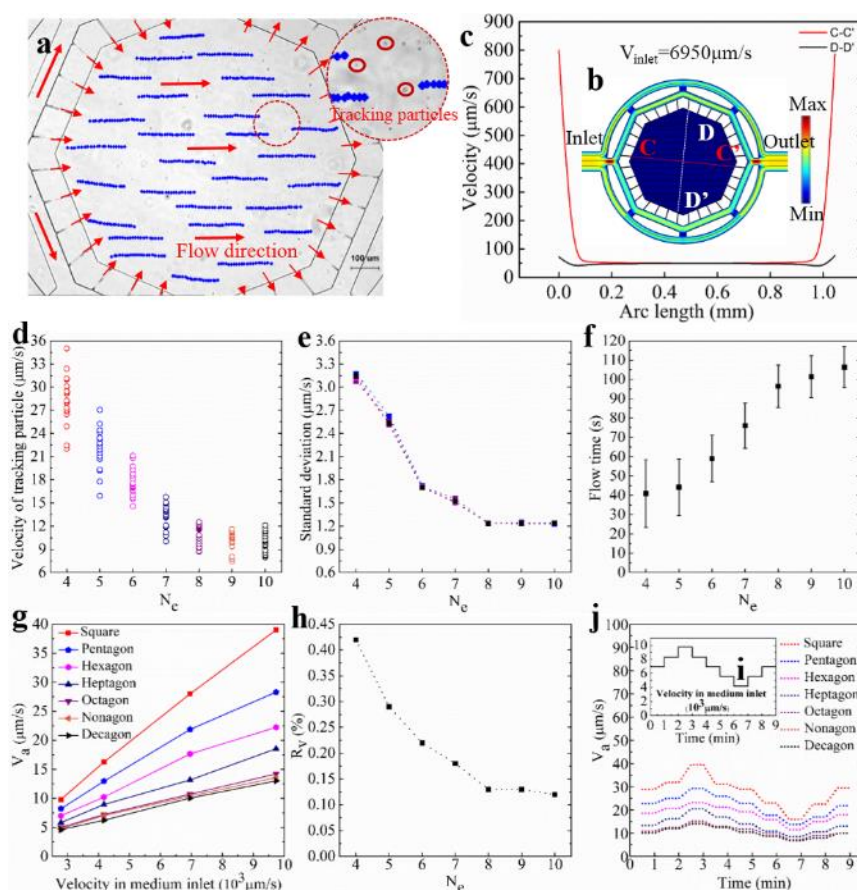
Fig. 4 The flow behaviour and the influence of chamber shape on uniformity and stability of the flow field in the chamber. (a)The moving trajectories of polystyrene (PS) microbeads in bio-inspired octagonal chamber; the moving direction of particles are in accordance with the flow direction of main channel; the blue line represents the trajectory of tracking particle; the red arrow represents the flow direction. (b) Velocity profile of the octagonal chamber simulated by Comsol 4.3a; the colour represent the velocity magnitude (the velocity becomes big from blue to red); C-C' and D- D' are cross-lines from one microgap inlet to one microgap outlet, the point C, C', D, D' are located at the joint of the microgaps and chamber. (c) The velocity profiles along the cross-line C-C' and D- D'. (d) The velocities of 20 picked PS microbeads in seven types of chambers under medium inlet velocity of 6950 μm/s. (e) The standard deviation of the 20 picked PS microbeads in seven types of chambers under medium inlet velocity of 6950 μm/s for four experiment times. (f) The average flow time of microbeads in seven types of chambers under medium inlet velocity of 6950 μm/s. (g) The average velocities in seven types of chambers vary with the velocity of medium inlet. (h) The relative velocity variations in chambers with different shapes. (i) The wave profile of medium inlet velocity. (j) The average velocities in seven types of chambers vary with the periodic fluctuations of the medium inlet velocity.

in Fig. 4d and Fig. 4e indicate that the flow fields in the polygonal chambers tend to become uniform and the velocity variations become small as the number of edges (N_e) increases. Furthermore, as N_e increases above 8, the change in flow fields will become less evident.

Flow time. The designed bionic devices can also meet the requirements of efficient medium exchange. To demonstrate such a feature, the medium exchange time, which is measures by the flow time of microbeads through the chamber, has been used and recorded. As is shown in Fig. 4f, the flow times in the chambers with different N_e (4, 5, 6, 7, 8, 9 and 10) are 40.86 ± 17.55 s, 44.17 ± 14.62 s, 59.05 ± 12.02 s, 76.05 ± 11.69 s, 96.39 ± 11.60 s, 101.45 ± 10.76 s, 106.35±10.57 s, respectively. This means that sufficient and fast medium exchange can be achieved in these polygonal chambers, which further proves that the designed bio-inspired chambers are able to provide a microenvironment that, the supply of cell culture medium and the removal of metabolic waste are efficient.

Minimizing in-vitro microenvironment disturbance. To demonstrate the capability of minimizing the external

disturbance on flow fields in the bio-inspired polygonal chambers, a set of initial injecting flow rates including 2 μl/min (2780 μm/s), 3 μl/min (4170 μm/s), 5 μl/min (6950 μm/s) and 7 μl/min (9730 μm/s) have been used. Fig. 4g shows the average velocity (V_a) in the polygonal chambers with different number of edges. It can be observed that as the inlet velocity changes from 2780 μm/s to 9730 μm/s, the V_a in the seven types of chambers exhibits a pronounced reduction when the number of edges in the polygonal chamber increases. As the number of edges increases from 4 to 8, the change of V_a (the maximum velocity subtract the minimum velocity) in the polygonal chambers have reduced nearly 68%, which indicates that the flow fields within a chamber with more edges is more stable. It is due to that the more edges means more flow paths, which can provides alternative routes to accommodate external disturbance. As the number of edges increases to 9 and 10, the changes of V_a are 8.8 μm/s and 8.4 μm/s respectively, which is not obviously compared to that of octagonal chamber (9.2 μm/s). It indicates that the flow fields within a polygonal chamber can be retained relative steady if the number of edges

is more than 8. This is because that the bio-inspired octagonal chamber has enough redundancy to minimize this level of external disturbance. We also use the relative velocity variation (R_v), which is defined as the ratio of the average velocity variation to the variation of inlet velocity, to evaluate the stability of the flow velocity within the bio-inspired polygonal chambers. It can be found that the R_v in these seven bio-inspired chambers are all very small (Fig. 4h), which means that the bionic design has inherent function to reduce the external disturbance. This means that the large amount of microgaps on the wall of the chambers can also increase the redundancy of the chambers. Further, the smaller R_v, the more stable the flow velocity within a chamber. It can be observed that R_v reaches the minimum value as the number of edges increases over 8, which also reveals that the changes of flow field in a chamber becomes less severe if more than 8 edges is applied.

We also measured the changes of flow field in the chambers subject to different shapes as the velocity in the medium inlet is pulsatile, which is in common with the flow in the blood vessels. The pulsatile flow rate is programmed on the syringe pump and the velocity profile in medium inlet is shown in Fig. 4i (placed inside Fig. 4j). The pulsation period is 8 min. The range of the medium inlet velocity changes from 4170 µm/s to 9730 µm/s, and the change is 1390 µm/s every minute. The average velocities (V_a) in different chambers in one period are shown in Fig. 4j. Because the geometries of microgaps and the size of chambers are identical in these seven type of chambers, the average velocity (V_a) in the chamber will only be affected by the number of edges in the polygonal chambers. Fig. 4j shows that the variations of V_a in these chambers have the similar tendency with the velocity profile of medium inlet, where the maximum occurs in the third minutes and the minimum in the seventh minutes. It can be seen that when the number of edges reaches 8, the velocity curve in one period tends to gentle. These experimental results are in accordance with botanical theoretical analysis in the section of 'Principle'.

Effects of microgap geometry on flow field in chamber

In a plant leaf, the large amount of pits that are responsible for liquid exchange[33] can increase the redundancy and stability of flow field. For our device, the microgaps have been used to mimic the pits, and the effects of the number and size of microgaps on the flow fields within an octagonal chamber have been investigated.

First, we study the effects of the number of microgaps (N_m). Different devices have been fabricated with N_m being 2, 4, 8, 16, 24, 32, 40 and 48. And the size of microgaps of all the devices being kept the same as 6µm. PS microbeads suspension with a concentration of 0.01% are injected into the devices and the velocity in the medium inlet is 6950 µm/s. The trajectories of the PS microbeads are recorded. Twenty microbeads which distribute uniformly in the chamber are picked as the tracking particles. Their trajectories and velocities are analysed by using the track object model in Image Pro Plus software (ESI† Fig. S6). The coefficient of variation (C_v), which is defined as the ratio of standard deviation to average, is used to estimate the effects of N_m on the flow field within the octagonal chambers. A smaller

C_v means the flow field is more uniform. The experimental results are shown in Fig. 5a. As the N_m increases from 2 to 32, C_v reduces 81% from 0.58 to 0.11, which indicates that the flow fields will be more uniform when the number of microgaps increases. Furthermore, as N_m increases from 32 to 48, C_v changes slightly, which indicates that the effects of N_m on flow fields will become small as it increases above 32. Our results have shown that, with the increase in N_m, the flow fields within a polygonal chamber becomes steady and gentle.

In addition, the change in N_m also can affect the efficiency of medium exchange in the polygonal chamber. The flow time of the microbeads from moving into the chamber to out of the chamber has also been measured, and the results are shown in Fig. 5b. It can be seen that the flow time has been reduced nearly 300s as N_m increases from 2 to 32, which means that the medium exchange efficiency has been improved significantly.

Second, we analyse the influence of the circumferential width of microgaps on the flow field within the octagonal chamber. Five types of circumferential widths, i.e. 5 µm, 6 µm, 7 µm, 9 µm and 11 µm, are used in the experiments. The velocities in the medium inlet are adjusted as the external disturbance and the changes of the average velocities (V_a) within the chambers with different microgap width are measured using the particle tracking technique (ESI† Fig. S7). Results are shown in Fig. 5c. The maximal velocity change can be observed in the chamber with 11 µm-wide microgaps. In this case, V_a increases more than 8.4-folds with the velocity in the medium inlet changing from 2780 µm/s to 9730 µm/s. When the width of microgap is 9 µm, the increase in V_a is nearly 6.7-folds. However, when the width of microgap is below 7µm, the increase in V_a is less than 3.3-folds. It indicates that the capability of the polygonal chamber to minimize the external disturbance will decrease as the widths of microgaps increase. The reason is that the flow resistance will increase when the size of microgaps decreases, as a result, the velocity in the chamber will decrease accompanied with the decrease of the change of velocity.

Influences of chamber size on flow field in chamber

The area of areole will affect the water transportation.[34] In the leaves of dicotyledonous plants, the sizes of areoles are diverse. To investigate the effects of chamber size on flow fields, we designed four different types of octagonal chambers with different inscribed circle diameter (D_i), i.e. 500 µm, 1000 µm, 1500 µm and 2000 µm. The number of microgaps is kept at 32 with the circumferential width of the microgaps being 6 µm. The fluid velocities in these chambers are measured by using the tracking particle technique (ESI† Fig. S8). To study the influence of chamber size on uniformity of the flow field in chamber, the velocity in the medium inlet is set to be 6950 µm/s. The coefficient of velocity variation (C_v) is calculated with the results shown in Fig. 5d. It can be seen that there is a minimum value of C_v when D_i is 1000 µm indicating that the velocities in the chamber with D_i of 1000 µm is more uniform than the others. Hence, 1000 µm is the optimal size of the chamber in order to make a uniform flow field for cell culture.
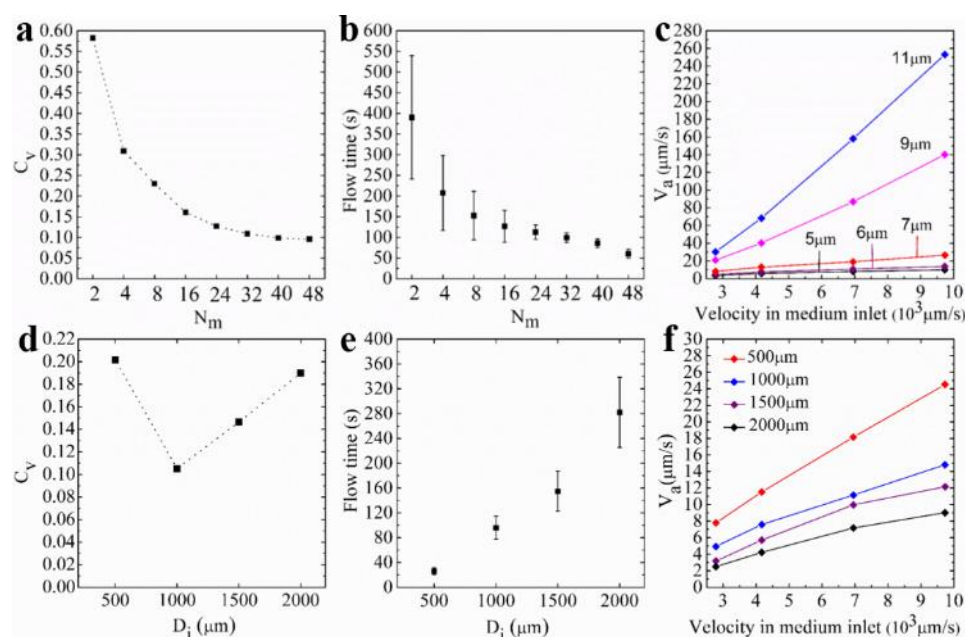
Fig. 5 The influences of the number of microgaps, gap size and chamber size on flow fields in chambers. (a) The coefficient of velocity variation (standard deviation/average) in chamber varies with the number of microgaps. (b) The flow times in chambers of different gap numbers. (c) The average velocities in chambers of different gap size vary with the velocity of medium inlet. (d) The coefficient of velocity variation (standard deviation/average) in chamber varies with chamber size. (e) The flow times in chambers of different chamber size. (f) The average velocities in chambers of different chamber size vary with the velocity of medium inlet.

Another important affect brought from the size of chamber is the efficiency of the medium exchange. To study such a relationship, the flow time of PS microbead from entering to leave the chamber has been recorded, as shown in Fig. 5e. For the chamber with D_i of 500 μm, 1000 μm, 1500 μm and 2000 μm, the flow time is 25.85 ± 5.59 s, 96.20 ± 18.67 s, 154.92 ± 31.94 s, 282.08 ± 56.54 s, respectively.

Finally, the influences of chamber size on minimizing external disturbance have also been estimated, which is shown in Fig. 5f. The velocity variation is 16.7 μm/s for the chamber with D_i of 500 μm as the velocity in medium inlet changes from 2780 μm/s to 9720 μm/s, while the velocity variation is less than 10μm/s when Di exceeds 1000 μm. These results indicate that the chamber with inscribed circle diameter more than 1000 μm has the better performance on minimizing the external influence.

Cell culture

Most of the in-vivo cells live in the tissue. The fluid flow in tissue is interstitial flow, which is in constant motion and the velocity is extremely slow.[9] It is typically assumed that the velocity ranges from 0.1 μm/s to 10 μm/s for tumors.[10] The results of the particle tracking experiments mentioned above are able to prove that the bio-inspired microfluidic devices could control the velocities in the cell culture chambers to the required level of interstitial flow, and the redundant microchannels could provide multi-paths to resist the external disturbances. Besides, the velocities in most region of the chamber are uniform, which can guarantee the fluid microenvironments of most of cells are the same. To investigate the performance of the bio-inspired devices, three types of cells, i.e. Hela cells, PC-12 cells and HUVEC cells are cultured. The control octagonal device without

redundant structures (ESI† Fig. S9a) and the culture dish are used as the control group (as shown in Fig. 6a-6c).

Shear stress. In the experiment of investigating the flow fields in the bio-inspired polygonal chambers with different shapes, we observed that the moving directions of the tracking particles are aligned with the directions of microgaps when they entering the chambers, then the moving directions become consistent with the flow directions in the main channels. Thus, the flow in the chambers can be regard as the pressure-driven flow between two parallel plates. Under the medium inlet velocity of 6950 μm/s, the average velocities on the semi-heights of chambers with different shapes have been measured by using the particle tracking technique, which can assist with calculating the velocities on the semi-height of cells and the shear stress on the bottom of chambers. In Fig. 6d, it can be observed from the velocity profile that the velocities on the semi-height of cells have the same magnitude with the interstitial flow. Besides, the velocities inside the polygonal chambers decrease as the increase of the number of edges. From the wall shear stress curve, it can be seen that the shear stress on the bottom of chambers also decrease as the increase of the number of edges of a polygonal chamber. And the shear stress can be very small (10^{-2}–10^{-4} dyne/cm^2).[35]

Normalized cell density. To study the effects of fluid flow on cell proliferation, the normalized cell densities (the initial cell numbers are all normalized to the level of culture dish) of Hela cells have been measured within 78h. The normalized cell densities in culture dish, control octagonal device, bio-inspired square device, bio-inspired hexagonal device, bio-inspired octagonal device and bio-inspired decagonal device are shown in Fig. 6e. It can be seen that the densities of cells increase rapidly between 30h and 54h, which are consistent with
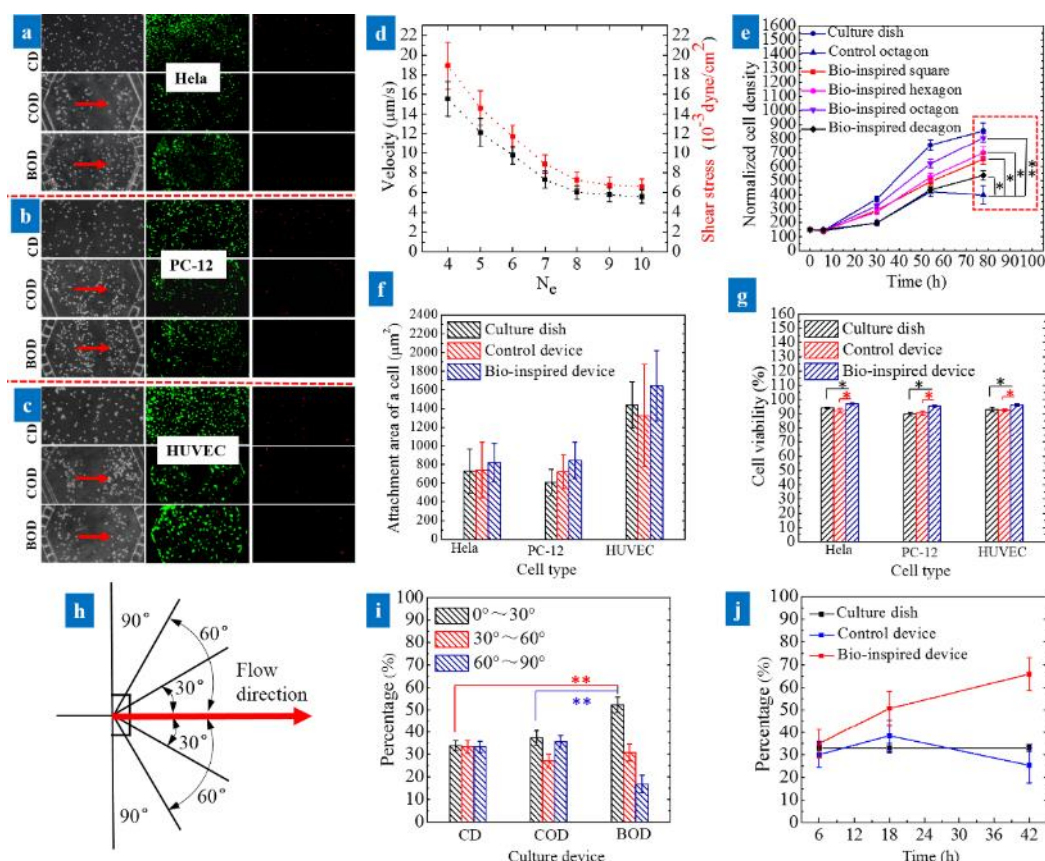
Fig. 6 Cell culture. (a) The Hela cells are cultured in culture dish (CD), control octagonal device (COD) and bio-inspired octagonal device (BOD). The red arrow is the flow direction of culture medium. The cells were stained by live (green)/dead (red) after culturing for 78 hours. (b) The PC-12 cells are cultured in culture dish (CD), control octagonal device (COD) and bio-inspired octagonal device (BOD). The red arrow is the flow direction of culture medium. The cells were stained by live (green)/dead (red) after culturing for 78 hours. (c) The HUVEC cells are cultured in culture dish (CD), control octagonal device (COD) and bio-inspired octagonal device (BOD). The red arrow is the flow direction of culture medium. The cells were stained by live (green)/dead (red) after culturing for 78 hours. (d) The velocity on the semi-height (5μm) of cells and the shear stress on the bottom of chambers with different shapes under the medium inlet velocity of 6950 μm/s. (e) The normalized cell densities of Hela cells in culture dish, control octagonal device, bio-inspired square device, bio-inspired hexagonal device, bio-inspired octagonal device and bio-inspired decagonal device change with culture time. The * and ** indicate statistical significance (P<0.05), (n=5) and (P<0.01), (n=5) respectively. (f) The average attachment area of a single cell after culturing for 30 hours in the culture dish (CD), control octagonal device (COD) and bio-inspired octagonal device (BOD). Three types of cells, including Hela, PC-12 and HUVEC are analyzed. (g) Cell viabilities are assessed by calculating the ratio of the number of live cells and the number of total cells in the culture dish (CD), control octagonal device (COD) and bio-inspired octagonal device (BOD). The * indicates statistical significance (P<0.05), (n=4). Three types of cells, including Hela, PC-12 and HUVEC are analysed. (h) The metric of cell alignment with the flow direction. (i) The percentage of PC-12 cell distribution in different angle after culturing for 18h. The red and blue ** indicate statistical significance (P<0.01), (n=4). (j)The percentage of PC-12 cell distribution in 0°～30° angle with flow direction varying with culture time.

standard s-shape cell growth curves. As the culture time is under 54h, the relative cell growth rates ($(N_A-N_B)/N_B$, where N_A is the cell number at time A, N_B is the cell number at time B, and A>B) has reached 403% in culture dish, which is higher than that in microfluidic devices (179% in control octagonal device, 227% in bio-inspired square device, 249% in bio-inspired hexagonal device, 313% in bio-inspired octagonal device and 189% in bio-inspired decagonal device). As the culture time increases above 54h, the relative cell growth rates in the bio-inspired microfluidic devices are larger than 24% which is obviously higher than that in culture dish (14%). The culture dish can promote the cell proliferation in some extent, but the metabolic waste would also accumulate in the culture dish, whose effects on the cell health may become obvious in a long-time culturing process. In addition, the static culture microenvironment is different from in-vivo, which may result in an incorrect analysis. The bio-inspired microfluidic cell culture device could control the flow velocity in the culture chamber, which can provide a balance between the accumulating of

endogenous growth factor[36, 37] and the removing of metabolic waste.

The average relative cell growth rates within 78h in control octagonal device, bio-inspired square, bio-inspired hexagonal, bio-inspired octagonal and bio-inspired decagonal devices are 165%, 335%, 365%, 437% and 260%, respectively. It can be found that the rates in bio-inspired devices are higher than that in control octagonal device. The reason is that the velocity in the control octagonal device is larger than that in the bio-inspired devices. The non-uniformity of velocity in the control octagonal device would also affect the growth of cells. Fig. 6e also indicates that the relative cell growth rate will increase as the edge number of bio-inspired chamber increases from four to eight. But it increases slowly in the bio-inspired decagonal chamber, which may be caused by the insufficient supply of the nutrition and the space for cell growth in this chamber. The T-Test results of normalized cell density at 78h mean that the bio-inspired chambers is more suitable for long time cell culture.

To further demonstrate the effects of flow fields in the bio-inspired device and control device on cell proliferation, we have reduced the average velocity in the control octagonal chamber to the magnitude of bio-inspired octagonal chamber. According to the simulation results, the flow rate in medium inlet of the control device requires to be reduced to 0.28 ul/min. The experimental results indicate that the bio-inspired octagonal device with medium inlet flow rate of 5 ul/min works obviously better than the control octagonal device (with medium inlet flow rate of 5 ul/min or 0.28 ul/min) in improving cell proliferation(as shown in ESI† Fig. S10a-d).

Attachment area of a single cell. The average attachment area of a single cell after culturing for 30 hours in the culture dish (CD), control octagonal device (COD), bio-inspired octagonal device (BOD) are shown in Fig. 6f. The results of Hela cells show that the average attachment area of a single cell in microfluidic devices (including COD and BOD) are larger than that in culture dish. The average attachment area of a single cell in the bio-inspired device is 819 μm^2 which is larger than that in the control octagonal device (738 μm^2). The results of PC-12 cells have the same tendency with the Hela cells. The bio-inspired device has the largest attachment area, which is about 1.17-folds of the control octagonal device and 1.38-folds of the culture dish. For HUVEC cells, the attachment area in the bio-inspired device is larger than that in the culture dish. But the culture dish is larger than that in the control octagonal device, which is different with Hela cells and PC-12 cells. The attachment area in BOD is also largest, which is about 1.14-folds of CD and 1.24-folds of COD. These results indicate that the bio-inspired device is more beneficial to enhance the area of cell spreading.

The standard deviation (SD) of the attachment area of a single cell can reflect the difference in size of cells. The standard deviations in culture dish, control octagonal device, bio-inspired octagonal device are 233.43 μm^2, 296.18 μm^2, 207.14 μm^2 for Hela cells. For PC-12 cells, their SDs are 138.86 μm^2, 182.19 μm^2, 142.87 μm^2 respectively. For HUVEC cells, their SDs are 248.63 μm^2, 547.32 μm^2, 375.39 μm^2 respectively. It can be found that the difference in sizes of cells in bio-inspired octagonal device is close to culture device, and better than control octagonal device, which indicates that a stable and uniform flow field can be obtained in the bio-inspired device and it is beneficial to cell attachment.

To further demonstrate the effects of flow fields in the bio-inspired device and control device on cell attachment, the flow rate in medium inlet of the control octagonal device has been reduced to 0.28 ul/min. The experimental results of Hela cells are shown in ESI† Fig. S10e. The results of T-test (p＜0.05) indicate that both the bio-inspired octagonal device with medium inlet flow rate of 5 ul/min and the control octagonal device with medium inlet flow rate of 0.28 ul/min work better than the control octagonal device with medium inlet flow rate of 5 ul/min.

Cell viability. After culturing for 78 hours, the cells in culture dish, control octagonal device and bio-inspired octagonal device are dyed by FDA/PI (live/Dead, Solarbio, Beijing, China). Fig. 6a-6c show the results of live/dead stain of Hela cells, PC-12 cells and HUVEC cells respectively. After staining for 15min, the live cells present green fluorescence, while the dead cells present red fluorescence. The cell viability has been evaluated by calculating the ratio of number of live cells and number of total cells. The cell viability in the culture dish, control octagonal device, bio-inspired octagonal device are 94.1%, 92.2%, 96.9% for Hela cells, 89.9%, 90.6%, 95.4% for PC-12 cells, 92.9%, 92.3%, 96.2% for HUVEC cells (Fig. 6g). The T-test results indicate that the cell viability in bio-inspired octagonal device has statistical significance compared to the cell viability in culture dish and control device.

Alignment of PC-12 cells. The interstitial flow has been reported to affect the morphology of cells.[38, 39] The results of particle tracking experiments in the study indicate that the bio-inspired device can control the flow field inside the culture chamber comparable to interstitial flow. In order to investigate the influences of the interstitial-like flow on cell alignment, PC-12 cells are cultured in the bio-inspired octagonal device (BOD). The culture dish (CD) and control octagonal device (COD) are used as comparisons. The streamlines inside the chambers of bio-inspired octagonal device (BOD) and control octagonal device (COD) are shown in ESI† Fig. S11a and S11b. It can be seen that the streamlines in the bio-inspired octagonal chamber are parallel with the flow direction in the main channel, and the streamlines in the control octagonal chamber present to be circular arc. The cells are cultured in static for 6h after seeding into the culture devices, then the PC-12 cells in BOD and COD are cultured dynamically with the medium inlet flow rate of 5μl/min for 36h. The state of cells are recorded after culturing for 18h and 42h (as shown in ESI† Fig. S11c-e). The streamline alignment metric is a measure of alignment bias along the streamlines, i.e. the absolute value of angle between the long axis of PC-12 cell and flow direction (as shown in Fig. 6h). The statistical results of the angles of cell alignment with flow direction after culturing dynamically for 12h are shown in Fig. 6i. It indicates that the angle distribution of cell alignment in culture dish (CD) is uniform. The percentage of angle distribution in control octagonal device (COD) between 0° and 30° is 37.4% ± 3.2%, while 52.3% ± 3.3% in bio-inspired octagonal device (BOD). The results of T-test (p＜0.01) indicate that the effects of interstitial-like flow in bio-inspired device on PC-12 alignment is obvious. Furthermore, with the increase of dynamic culturing time, the percentage of angle distribution in BOD between 0°and 30°increase to 65.8% ± 7.2% at time of 42h (as shown in Fig. 6j). The results indicate that the bio-inspired device could provide an elegant approach to place cells in interstitial flows.

Conclusions

The leaf venation is considered to be an optimal architecture for water transportation selected by nature, and one of the remarkable characteristics of leaf venation is the existence of multiple flow paths that maintain the flow of water to mesophyll under moderate levels, which is called redundancy. Inspired by the redundancy structures of leaf venation, we have

developed a series of chambers to investigate the influence of these structures on the flow fields in these chambers. The microchannels imitate the vessels in the leaf venation to transport cell medium, the cell culture chamber imitates the areoles of mesophyll and the microgaps between micropillars imitate the pits on the side walls of the vessels. The particle tracking technique has been applied to evaluate the flow field of the chambers. The experimental results indicate that the shape of chambers, the geometry of microgaps and the size of chambers all have influence on the flow fields in chambers. It can be concluded as follows: (1) The flow fields will become uniform and stable with the increase of the number of edges in the bio-inspired polygonal chamber, and the effect will become less evident when the number of edges reach to 8. These phenomenon are in accordance with botanical theoretical analysis. (2) The number of microgaps will affect the velocity uniformity in the chamber and the size of microgaps will influence the stability in the chamber. The velocity uniformity increases with the increase of the number of microgaps and the stability in the chamber decreases with the increase of the size of microgaps. (3) The size of chambers can be optimized to obtain the uniform and stable flow fields. For example, the bio-inspired octagonal chamber with inscribed circle diameter of 1000μm perform well when the number of microgaps is 32 and the size of microgaps is 6μm. In addition, the cell culture experimental results also support that the bio-inspired devices are beneficial to the growth and attachment of cells. In conclusion, the bio-inspired chamber can provide a dynamic, uniform and stable microenvironment for cells. Since the bio-inspired octagonal chamber has robust performances, it can be integrated in various cell manipulation microfluidic systems.

Conflicts of interest

There are no conflicts of interest to declare.

Acknowledgements

References

1   D. Gao, H. Liu, Y. Jiang and J. M. Lin, *Trends in Analytical Chemistry*, 2012, **35**, 150-164.
2   G. B. Saliebbeugelaar, G. Simone, A. Arora, A. Philippi and A. Manz, *ANAL CHEM*, 2010, **82**, 4848-4864.
3   E. W. Esch, A. Bahinski and D. Huh, *NAT REV DRUG DISCOV*, 2015, **14**, 248-260.
4   M. Mehling and S. Tay, *CURR OPIN BIOTECH*, 2014, **25**, 95.
5   E. K. Sackmann, A. L. Fulton and D. J. Beebe, *NATURE*, 2014, **507**, 181-189.
6   S. Halldorsson, E. Lucumi, R. Gómezsjöberg and R. M. Fleming, *Biosensors & Bioelectronics*, 2015, **63**, 218.
7   A. Rosenthal, A. Macdonald and J. Voldman, *BIOMATERIALS*, 2007, **28**, 3208-3216.
8   G. Pagano, M. Ventre, M. Iannone, F. Greco, P. L. Maffettone and P. A. Netti, *BIOMICROFLUIDICS*, 2014, **8**, 46503.
9   J. Y. Park, J. B. White, N. Walker, C. H. Kuo, W. Cha, M. E. Meyerhoff and S. Takayama, *BIOMICROFLUIDICS*, 2011, **5**, 2787.
10 J. M. Munson and A. C. Shieh, *Cancer Management & Research*, 2014, **6**, 317.
11 H. Li, J. Ma, Z. Hou and H. Xin, *ACTA PHYS-CHIM SIN*, 2008, **24**, 2203-2206.
12 M. A. Lopes, K. E. Lee, A. V. Goltsev and J. F. Mendes, *Physical Review E Statistical Nonlinear & Soft Matter Physics*, 2014, **90**, 52709.
13 S. M. Bonk, M. Stubbe, S. M. Buehler, C. Tautorat, W. Baumann, E. D. Klinkenberg and J. Gimsa, *Biosensors*, 2015, **5**, 513-536.
14 Y. C. Chen, P. Ingram and E. Yoon, *ANALYST*, 2014, **139**, 6371-6378.
15 F. M. Faraci, J. Choi, G. L. Baumbach, W. G. Mayhan and D. D. Heistad, *CIRC RES*, 1989, **65**, 417-425.
16 C. Luo, X. Zhu, T. Yu, X. Luo, Q. Ouyang, H. Ji and Y. Chen, *Biotechnology & Bioengineering*, 2008, **101**, 190-195.
17 K. Liu, R. Pitchimani, D. Dang, K. Bayer, T. Harrington and D. Pappas, *Langmuir the Acs Journal of Surfaces & Colloids*, 2008, **24**, 5955-5960.
18 P. J. Lee, P. J. Hung, V. M. Rao and L. P. Lee, *Biotechnology & Bioengineering*, 2006, **94**, 5-14.
19 B. Zhang, M. C. Kim, T. Thorsen and Z. Wang, *BIOMED MICRODEVICES*, 2009, **11**, 1233-1237.
20 C. Liu, L. Wang, Z. Xu, J. Li, X. Ding, Q. Wang and C. Y. L, *Journal of Micromechanics & Microengineering*, 2012, **22**, 65008-65014.
21 P. J. Hung, P. J. Lee, P. Sabounchi, N. Aghdam, R. Lin and L. P. Lee, *LAB CHIP*, 2005, **5**, 44-48.
22 H. Doméjean, L. M. S. P. De, A. Funfak, N. Atrux-Tallau, K. Alessandri, P. Nassoy, J. Bibette and N. Bremond, *LAB CHIP*, 2017,**17**, 110-119.
23 T. Nelson and N. Dengler, *PLANT CELL*, 1997, 9, 1121.
24 B. Blonder, C. F. De, J. Moore, M. Rivers and B. J. Enquist, *NEW PHYTOL*, 2012, **196**, 1274-1282.
25 F. E. Rockwell, N. M. Holbrook and A. D. Stroock, *J THEOR BIOL*, 2014, **340**, 267.
26 T. S. Field and T. J. Brodribb, *NEW PHYTOL*, 2013, **199**, 720.
27 L. Sack, E. M. Dietrich, C. M. Streeter, D. Sánchez-Gómez and N. M. Holbrook, *P NATL ACAD SCI USA*, 2008, **105**, 1567.
28 M. A. Zwieniecki, P. J. Melcher, C. K. Boyce, L. Sack and N. M. Holbrook, *Plant Cell & Environment*, 2002, **25**, 1445-1450.
29 F. Corson, *PHYS REV LETT*, 2010, **104**, 48703.
30 C. A. Price and J. S. Weitz, BMC PLANT BIOL, 2014, **14**, 234.
31 B. Blonder, C. Violle, L. P. Bentley and B. J. Enquist, *ECOL LETT*, 2011, **14**, 91.
32 K. Awumah, I. Goulter and S. K. Bhatt, *Stochastic Hydrology & Hydraulics*, 1990, **4**, 309-320.
33 B. Choat, A. R. Cobb and S. Jansen, *NEW PHYTOL*, 2008, **177**, 608.
34 W. A. Green, S. A. Little, C. A. Price, S. L. Wing, S. Y. Smith, B. Kotrc and G. Doria, *Applications in Plant Sciences*, 2014, **2**, 8.
35 J. Y. Park, S. J. Yoo, L. Patel, S. H. Lee and S. H. Lee, *BIORHEOLOGY*, 2010, **47**, 165.
36 H. Yu, C. M. Alexander and D. J. Beebe, *LAB CHIP*, 2007, **7**, 388-391.
37 S. Giulitti, E. Magrofuoco, L. Prevedello and N. Elvassore, *LAB CHIP*, 2013, **13**, 4430.
38 W. J. Polacheck, J. L. Charest and R. D. Kamm, *P NATL ACAD SCI USA*, 2011, **108**, 11115-11120.
39 J. Y. Park, S. J. Yoo, C. M. Hwang and S. H. Lee, *LAB CHIP*, 2009, **9**, 2194-2202.